$InsP_7$ is a small-molecule regulator of NUDT3-mediated mRNA decapping and processing-body dynamics

Soumyadip Sahu[a], Zhenzhen Wang[a], Xinfu Jiao[b], Chunfang Gu[a], Nikolaus Jork[c,d], Christopher Wittwer[c,d], Xingyao Li[a], Sarah Hostachy[e], Dorothea Fiedler[e], Huanchen Wang[a], Henning J. Jessen[c,d], Megerditch Kiledjian[b], and Stephen B. Shears[a,1]

[a]Signal Transduction Laboratory, National Institute of Environmental Health Sciences, NIH, Research Triangle Park, NC 27709; [b]Department of Cell Biology and Neuroscience, Rutgers University, Piscataway, NJ 08854; [c]Institute of Organic Chemistry, University of Freiburg, 79104 Freiburg, Germany; [d]Centre for Integrative Biological Signalling Studies, University of Freiburg, 79104 Freiburg, Germany; and [e]Department of Chemical Biology, Leibniz-Forschungsinstitut für Molekulare Pharmakologie, 13125 Berlin, Germany

Edited by Solomon H. Snyder, Johns Hopkins University School of Medicine, Baltimore, MD, and approved June 9, 2020 (received for review December 18, 2019)

Regulation of enzymatic 5′ decapping of messenger RNA (mRNA), which normally commits transcripts to their destruction, has the capacity to dynamically reshape the transcriptome. For example, protection from 5′ decapping promotes accumulation of mRNAs into processing (P) bodies—membraneless, biomolecular condensates. Such compartmentalization of mRNAs temporarily removes them from the translatable pool; these repressed transcripts are stabilized and stored until P-body dissolution permits transcript reentry into the cytosol. Here, we describe regulation of mRNA stability and P-body dynamics by the inositol pyrophosphate signaling molecule 5-$InsP_7$ (5-diphosphoinositol pentakisphosphate). First, we demonstrate 5-$InsP_7$ inhibits decapping by recombinant NUDT3 (Nudix [nucleoside diphosphate linked moiety X]-type hydrolase 3) in vitro. Next, in intact HEK293 and HCT116 cells, we monitored the stability of a cadre of NUDT3 mRNA substrates following CRISPR-Cas9 knockout of *PPIP5Ks* (diphosphoinositol pentakisphosphate 5-kinases type 1 and 2, i.e., *PPIP5K* KO), which elevates cellular 5-$InsP_7$ levels by two- to threefold (i.e., within the physiological rheostatic range). The *PPIP5K* KO cells exhibited elevated levels of NUDT3 mRNA substrates and increased P-body abundance. Pharmacological and genetic attenuation of 5-$InsP_7$ synthesis in the KO background reverted both NUDT3 mRNA substrate levels and P-body counts to those of wild-type cells. Furthermore, liposomal delivery of a metabolically resistant 5-$InsP_7$ analog into wild-type cells elevated levels of NUDT3 mRNA substrates and raised P-body abundance. In the context that cellular 5-$InsP_7$ levels normally fluctuate in response to changes in the bioenergetic environment, regulation of mRNA structure by this inositol pyrophosphate represents an epitranscriptomic control process. The associated impact on P-body dynamics has relevance to regulation of stem cell differentiation, stress responses, and, potentially, amelioration of neurodegenerative diseases and aging.

P bodies | cellular homeostasis | inositol | signaling

Removal (i.e., "decapping") of the 5′-end 7-methylguanosine (m^7G) cap of messenger RNAs (mRNAs) (Fig. 1*A*) can be a key event for reshaping the transcriptomic landscape in response to changing cell requirements (1). Decapping exposes the mRNA 5′ end to exonuclease-mediated degradation; this decay pathway plays critical roles in early animal development, cell growth and proliferation, immune response, and mRNA quality control (1). Among the four known classes of mammalian 5′-decapping enzymes there is one in which the unifying feature is the nucleoside diphosphate linked moiety X (Nudix) consensus catalytic sequence $GX_5EX_7REUXEEXGU$, where U represents a hydrophobic residue and X represents any amino acid; the Nudix-type decapping enzymes are DCP2, Nudix-type hydrolase 16 (NUDT16), and Nudix-type hydrolase 3 (NUDT3) (2, 3). Each of these enzymes preferentially decaps a subset of mRNAs. For example, NUDT3 specifically targets a small subset of mRNAs that are preferentially promigratory transcripts (2, 4).

The characterization of modulatory compounds that might control decapping could considerably illuminate our understanding of the regulation of gene expression. Here we describe regulation of NUDT3-catalyzed decapping by the most abundant member of the inositol pyrophosphate (PP-InsP) signaling family, 5-diphosphoinositol pentakisphosphate (5-$InsP_7$; Fig. 1*B* and *SI Appendix*, Fig. S1). 5-$InsP_7$ has already received considerable attention for a number of separate biological effects (5), many of which have been interpreted as acting at the interface of signaling and metabolic homeostasis (6). Consequently, 5-$InsP_7$ is pivotal to an organism's ability to adapt to environmental challenges—that is, its long-term survival—which is reliant upon dynamic control over uptake, storage, and utilization of various metabolic fuels (7). 5-$InsP_7$ also operates as a bioenergetic sensor, with its levels responding rapidly to changes in adenosine triphosphate (ATP) levels within the physiological range (8, 9).

NUDT3 was originally characterized (and named DIPP1) through its ability to dephosphorylate all PP-InsPs, including 5-$InsP_7$ (10). Here we describe our evidence that competition between 5-$InsP_7$ and 5′-capped mRNA for hydrolysis by NUDT3 impacts transcript levels in intact cells. This conclusion drew us to reports that inhibition of 5′ decapping is associated with

Significance

Improved understanding of the epitranscriptomic control process will help decipher regulation of global gene expression. Here, we demonstrate that the cell-signaling inositol pyrophosphate 5-$InsP_7$ stabilizes mRNAs that are normally committed to decay pathways by NUDT3-mediated removal of the protective 5′ cap. We demonstrated this effect of 5-$InsP_7$ in vitro using recombinant NUDT3. Then, we applied pharmacological, genetic, and chemical tools to manipulate cellular levels of 5-$InsP_7$, thereby showing it to enhance mRNA stability in intact cells. We further demonstrate mRNA stabilization is paralleled by increased abundance of P bodies, which are membraneless condensates that sequester mRNAs from the translating pool. Our demonstration that 5-$InsP_7$ regulates mRNA structure and stability, as well as P-body dynamics, illuminates cell-signaling oversight of cellular homeostasis.

Author contributions: S.S., Z.W., C.G., H.W., M.K., and S.B.S. designed research; S.S., Z.W., X.J., C.G., and X.L. performed research; N.J., C.W., S.H., D.F., and H.J.J. contributed new reagents/analytic tools; S.S., Z.W., X.J., C.G., and S.B.S. analyzed data; and S.S., Z.W., S.H., D.F., H.J.J., M.K., and S.B.S. wrote the paper.

The authors declare no competing interest.

This article is a PNAS Direct Submission.

[1]To whom correspondence may be addressed. Email: shears@niehs.nih.gov.

This article contains supporting information online at https://www.pnas.org/lookup/suppl/doi:10.1073/pnas.1922284117/-/DCSupplemental.

First published July 29, 2020.

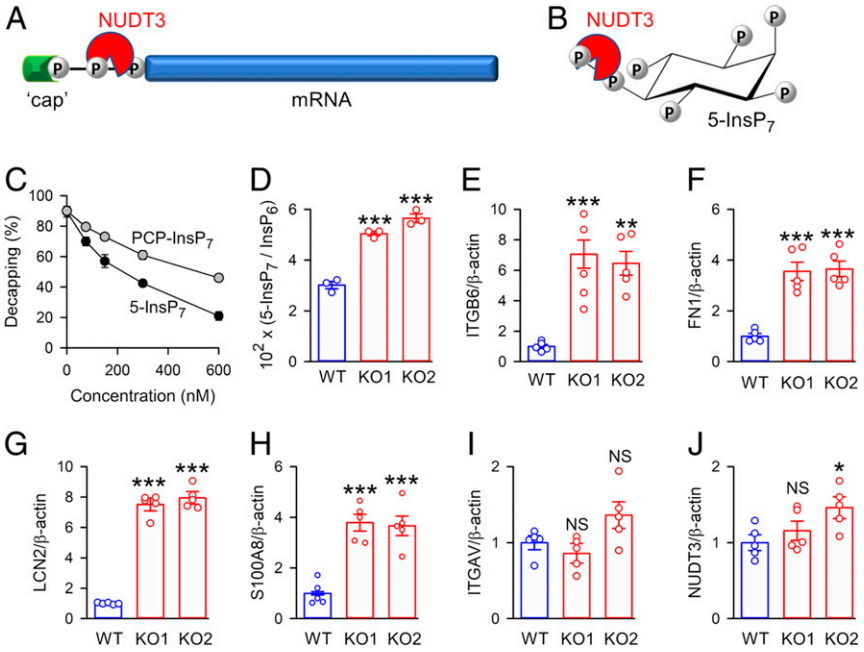

Fig. 1. Differential expression of selected RNA transcripts in WT and *PPIP5K* KO HEK293 cells, as a consequence of $InsP_7$ and the 5′-m^7G cap both being substrates for hydrolysis by NUDT3. (*A* and *B*) Graphically depicted hydrolysis by NUDT3 of phosphodiester bonds in the m^7G mRNA cap and $InsP_7$, respectively; in the former (*A*), cleavage of the βγ-diester is shown, but the enzyme also cleaves the αβ-diester (relative to the 5′-terminal guanine; *SI Appendix*, Fig. S2). (*C*) Dose-dependent inhibition of NUDT3-catalyzed 5′ decapping by either PCP-$InsP_7$ (gray circles), or 5-$InsP_7$ (black circles) or studied in vitro; means and SEs (when larger than the symbols) are shown for three or four biological replicates. (*D*) Levels of $InsP_7$ in WT cells (blue) and two independent clones (KO1 and KO2) of *PPIP5K* KO cells (red). (*E–J*) Levels of mRNA transcripts (ITGB6, FN1, LCN2, S100A8, ITGAV, and NUDT3, respectively) in WT cells (blue) and *PPIP5K* KO cells (red) as recorded by quantitative real-time PCR. Individual data, means, and SEs are shown for three or five biological replicates, as indicated. $*P < 0.05$, $**P < 0.02$, $***P < 0.001$, compared with WT. NS, not significant.

processing (P)-body accumulation (11, 12); the latter are highly dynamic, membraneless biomolecular condensates that sequester certain mRNAs (13). While the original concept that P bodies regulate mRNA decay continues to be pursued (12, 14), these organelles are now recognized as important sites for sequestration and storage of mRNAs away from the translating pool (15). Independent of transcription, the mRNAs in P bodies can be rapidly reintroduced into the translating pool, for example in response to certain environmental cues (12, 16, 17).

P bodies are increasingly recognized to have other functions. They transport mRNAs to localized sites of translation to ensure protein compartmentalization, for example to support synaptic plasticity in polarized neuronal cells; interest in this area extends to exploring possible roles of P bodies in neurodegenerative diseases (18, 19). The formation of P bodies is enhanced as part of the adaptive response to cell stress (12), and also during aging (20). Certain viruses manipulate P-body dynamics to counteract mRNA decay machinery (21). Dissolution of P bodies in embryonic stem cells and adult progenitors releases key fate-instructive mRNAs to drive cellular differentiation (22). It is therefore important to understand regulation of both the functions and the turnover of P bodies. We report here that P-body abundance parallels the 5-$InsP_7$–modulated levels of NUDT3-regulated mRNA transcripts.

Results and Discussion

Competition between 5-$InsP_7$ and the 5′-mRNA Cap for the Active Site of NUDT3. The 20-kDa NUDT3 protein was originally named DIPP1, due to its biologically relevant PP-InsP phosphatase activity (Fig. 1*B* and *SI Appendix*, Fig. S1) (10). In separate and more recent studies, NUDT3 was found to hydrolyze the triphosphate linker of the 5′-m^7G cap from a limited number of mRNAs (4, 23). Previously published biochemical, mutagenic, and structural data demonstrate that the single Nudix active site in NUDT3 hydrolyzes both substrates (4, 10, 24). Therefore, we anticipated these two substrates would compete for hydrolysis by NUDT3. This prediction was confirmed in assays performed with recombinant NUDT3 in vitro: 5′ decapping is inhibited by 5-$InsP_7$ with a half-maximal inhibitory concentration of ∼130 to 200 nM (Fig. 1*C* and *SI Appendix*, Fig. S2).

We also found that decapping in vitro is inhibited by the other PP-InsP substrates of NUDT3 (1-$InsP_7$ and $InsP_8$; *SI Appendix*, Figs. S1 and S2*C*). This is an expected result, since each of these PP-InsPs is hydrolyzed by NUDT3 with very similar kinetic parameters (25). Among the PP-InsPs, the inhibitory effect of 5-$InsP_7$ is the most likely to be physiologically relevant, based upon its cellular levels being 10- and 50-fold higher than those of $InsP_8$ and 1-$InsP_7$, respectively (26).

Decapping by NUDT3 is also inhibited in vitro by $InsP_6$ (*SI Appendix*, Fig. S2*C*), due to this inositol phosphate competitively inhibiting substrate binding to the catalytic site (10, 24). However, it is doubtful that inhibition of NUDT3 by $InsP_6$ is important in vivo, because it seems that only a minor fraction of total cellular $InsP_6$ is freely diffusible within the cytoplasm. For example, radiolabeling studies have shown that $InsP_6$ is compartmentalized between various subcellular pools (27). It has also been demonstrated that $InsP_6$ binds to cellular membranes (28). A significant proportion of cellular $InsP_6$ acts as a structural cofactor for proteins, and this immobilized ligand is not readily exchangeable with the cytosolic pool (29, 30). There are also indications that $InsP_6$ enters vesicular compartments in order to be dephosphorylated (31, 32).

In view of these complicating factors, we set out to analyze NUDT3 activity in intact cells, using experimental conditions in which we could manipulate levels of individual PP-InsPs in a controlled manner.

Expression of NUDT3 mRNA Substrates in Wild-Type and *PPIP5K* Knockout Cells. The knockout (KO) of *PPIP5K*s (diphosphoinositol pentakisphosphate 5-kinases type 1 and 2) in HEK293 cells leads to a stable, two- to threefold increase in 5-InsP_7 levels (Fig. 1*D*; data are shown for two clonal KO cell lines, designated "KO1" and "KO2"; also see ref. 9). In contrast, the KO cells cannot synthesize either 1-InsP_7 or InsP_8, while InsP_6 levels in KO cells remain at the levels observed in wild-type (WT) cells (*SI Appendix*, Fig. S1) (9). Thus, among those inositol phosphates that we have shown to inhibit mRNA decapping by NUDT3 in vitro (see above), 5-InsP_7 is the only one that shows an increase in its levels in *PPIP5K* KO cells. Thus, we have used these cells as a model for exploring if there is a role for 5-InsP_7 in regulating mRNA levels.

In order to monitor NUDT3 activity in intact cells, we assayed the levels of a cadre of its preferred substrates: mRNAs for integrin β6 (ITGB6), fibronectin (FN1), lipocalin-2 (LCN2), and S100 calcium-binding protein A8 (S100A8) (2, 4). These four transcripts were identified by RNA-sequencing analysis to be among those that were the most responsive (in terms of elevated levels) upon stable knockdown of NUDT3 in an MCF-7 breast cancer cell line (4). That phenotype was complemented by overexpression of WT NUDT3 but not by the decapping-deficient NUDT3$^{EE/QQ}$ mutant (4). The latter work has also contributed to the current consensus that mammalian cells contain multiple decapping enzymes that each control the stability and expression of distinct mRNA transcripts (2, 3).

Using quantitative real-time PCR, we found elevated levels of mRNA transcripts for ITGB6, FN1, LCN2, and S100A8 in *PPIP5K* KO HEK293 cells compared with WT cells (Fig. 1 *E*–*H*). It is of further significance that the WT and *PPIP5K* KO cells contain similar levels of the ITGAV mRNA transcript (Fig. 1*I*), which is not subject to 5′ decapping by NUDT3 (4). We also showed that the elevation in *PPIP5K* KO cells of the levels of mRNAs that are NUDT3 substrates is not due to a decrease in expression of NUDT3 itself (Fig. 1*J*).

These data are consistent with the hypothesis that NUDT3-mediated decapping is inhibited by the elevated levels of 5-InsP_7 in *PPIP5K* KO HEK293 cells. However, by themselves, these data do not exclude the alternate possibility that, through some

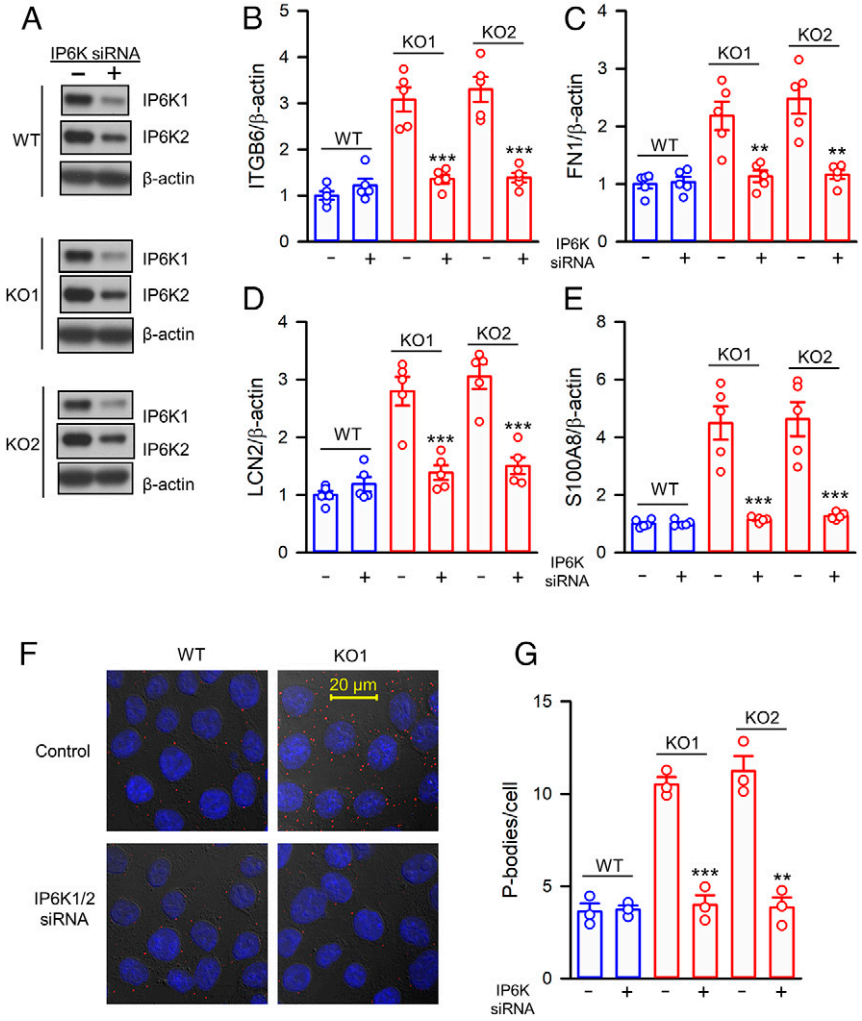

Fig. 2. Effects of IP6K knockdown on levels of mRNA transcripts and P-body abundance in WT and *PPIP5K* KO HCT116 cells. WT cells (blue) and two independent clones of *PPIP5K* KO cells (KO1 and KO2; red) were each treated with either control siRNA (minus sign) or IP6K(1 + 2) siRNA (plus sign), and then the following data were obtained from these cells. (*A*) Western assays of IP6Ks. (*B*–*E*) mRNA transcript levels for ITGB6, FN1, LCN2, and S100A8, respectively, determined by quantitative real-time PCR. (*F*) Representative merged, confocal wide-field images from bright-field, Hoechst staining (blue), and DCP1A immunofluorescence to tag P bodies (red). Individual data, means, and SEs are shown for five biological replicates. (*G*) P-body numbers per cell; in every biological replicate (three in total; means and SEs are shown), between 166 and 405 cells were analyzed from each of the six separate conditions. $^{**}P < 0.01$, $^{***}P < 0.001$, compared with WT.

unknown NUDT3-independent mechanism, 5-$InsP_7$ may affect P-body accumulation (see below) and indirectly stabilize those mRNAs which are normally decapped by NUDT3. This possibility is hard to exclude using most cell models, since NUDT3 knockdown and/or overexpression would be expected to impact levels of both 5-$InsP_7$ levels and those mRNA transcripts that are decapped by NUDT3. However, we have found an experimental system in which the 5′-decapping and 5-$InsP_7$ phosphatase activities of NUDT3 are uncoupled: the MCF-7 model in which NUDT3-mediated 5′ decapping was first established (see above). We used high-performance liquid chromatography analysis of [^{3}H]inositol-labeled WT and NUDT3 knockdown MCF-7 cells to quantify 5-$InsP_7$ levels, and found there was not a significant difference between the two cell lines ($P > 0.4$): WT cells, 5-[^{3}H]$InsP_7$, $3.9 \pm 0.6 \times 10^{-3}$ (relative to [^{3}H]$InsP_6$) and $1.2 \pm 0.2 \times 10^{-5}$ (relative to [^{3}H]inositol lipids), $n = 4$; the corresponding data for NUDT3 knockdown cells are $4.8 \pm 1 \times 10^{-3}$ and $1.4 \pm 0.2 \times 10^{-5}$, respectively. It is also notable that the levels of 5-$InsP_7$ in WT cells are almost 10-fold less than the usual value for mammalian cells (i.e., the corresponding value for HEK293 cells is $3.0 \pm 0.2 \times 10^{-2}$; Fig. 1*D*). In this context in which 5-$InsP_7$ levels are unchanged in MCF-7 cells upon NUDT3 knockdown, elevation in levels of specific mRNA transcripts [as previously reported (4)] is a phenomenon that is consistent with a reduction in NUDT3-mediated decapping.

We next monitored the rate of decay of our selection of mRNA substrates, by treating WT and KO cells with actinomycin D (ActD) (*SI Appendix*, Fig. S3). Data are presented relative to the β-actin mRNA, which was stable in all three cell lines (*SI Appendix*, Fig. S3*A*). Importantly, the rate of decay for the non–NUDT3-responsive ITGAV mRNA was comparable between KO1, KO2, and WT cell lines (*SI Appendix*, Fig. S3*B*). Moreover, each of the four transcripts that are decapped by NUDT3 (ITGB6, FN1, LCN2, and S100A8) were all significantly more stable following ActD addition to the two KO cell lines, as compared with WT cells (*SI Appendix*, Fig. S3 *C–F*). Our data indicate increased stability of mRNA substrates for NUDT3.

The increased stability of NUDT3-hydrolyzed mRNAs was not associated with a general, corresponding change in protein expression; only the ITGB6 and S100A8 proteins were expressed at higher levels in the KO lines (*SI Appendix*, Fig. S4 *A–D*). It is well-known from published proteogenomic analyses that mRNA and protein levels are often poorly correlated (33).

Our results are not specific to the HEK293 cell line. We have previously described our creation of two independent clones of *PPIP5K* KO HCT116 cells, in which levels of $InsP_7$ are also elevated (9). We found that these KO cells also expressed higher levels of mRNA transcripts for ITGB6, FN1, LCN2, and S100A8, as compared with WT cells (*SI Appendix*, Fig. S5 *A–D*). Again, the NUDT3 "negative control" is supportive of our hypothesis: *PPIP5K* KO did not affect levels of ITGAV mRNA (*SI Appendix*, Fig. S5*E*). As is the case with HEK293 cells, the increased transcript levels in *PPIP5K* KO HCT116 cells were not associated with a general elevation in the levels of expression of the corresponding proteins, with the exception of FN1 (*SI Appendix*, Fig. S5 *F–H*). While FN1 has a role in cell migration (34), there was not an effect of the KO upon wound healing (*SI Appendix*, Fig. S6).

Knockdown of $InsP_7$ Synthesis Decreases Levels of NUDT3 mRNA Substrates in *PPIP5K* KO Cells. To pursue the idea that it is a higher 5-$InsP_7$ concentration that promotes increased levels of NUDT3 mRNA substrates in *PPIP5K* KO cells, we used small interfering RNA (siRNA) to knock down IP6K-mediated 5-$InsP_7$ synthesis (*SI Appendix*, Fig. S1) (9). There are three IP6K isoforms, but type 3 IP6K is not expressed in HCT116 cells (35), so we knocked down IP6K1 and IP6K2 (Fig. 2*A*). This siRNA treatment of the KO cells reversed the elevation of levels of mRNA for ITGB6, FN1, LCN2, and S100A8 (Fig. 2 *B–E*). IP6K1/2 knockdown had similar effects upon the same transcripts in *PPIP5K* KO HEK293 cells (*SI Appendix*, Fig. S7).

P-Body Abundance Correlates with Modulation of NUDT3 Activity by $InsP_7$. There is increasing interest in reports that inhibition of 5′ decapping is associated with P-body accumulation (11, 12). We therefore studied P-body dynamics: Confocal immunofluorescence of the P-body marker DCP1A (36) showed that individual *PPIP5K* KO HCT116 cells contained ∼2.5-fold more P bodies per cell than did WT cells (Fig. 2 *F* and *G*). This increase in P-body abundance was fully reversed upon inhibition of $InsP_7$ synthesis by cell treatment with IP6K1/2 siRNA (Fig. 2 *F* and *G*). We also used a pharmacological approach to reduce cellular 5-$InsP_7$ accumulation (9, 37); we treated *PPIP5K* KO HCT116 and HEK293 cells with an IP6K inhibitor, N2-(*m*-trifluorobenzyl), N6-(*p*-nitrobenzyl) purine (TNP; *SI Appendix*, Fig. S1). TNP reduced expression of all four target mRNAs (Fig. 3 *A–D* and *SI Appendix*, Fig. S8), and decreased P-body abundance in both WT and *PPIP5K* KO cells (Fig. 3 *E* and *F*). Thus, we conclude that P-body abundance correlates with modulation of NUDT3 activity by 5-$InsP_7$.

To further pursue the role of 5-$InsP_7$ in regulating mRNA expression and P-body dynamics, we next used a liposomal delivery method which we recently developed to deliver PP-InsPs into cells (38). Here, we also investigated the efficiency of liposomal delivery of PP-InsP by using a fluorescein-tagged analog of 5-$InsP_7$ (FAM-$InsP_7$) (Fig. 4*A*). Subsequent extraction of the fluorescence-tagged molecule from cell lysates, and analysis by polyacrylamide gel electrophoresis (PAGE), revealed that the material eluted as a single band (*SI Appendix*, Fig. S9), indicating it was not significantly dephosphorylated; the bulky FAM group presumably gives protection to the normally metabolically labile 5-phosphate diester. Confocal analysis of cells loaded with FAM-$InsP_7$ indicated it was predominantly distributed throughout the cytoplasm (Fig. 4*B*). The FAM-$InsP_7$ was excluded from the nucleus, and only a minor proportion of FAM-$InsP_7$ associated with LysoTracker red (Fig. 4*B*), a marker for lysosomes/endosomes (weighted colocalization coefficient, 0.16 ± 0.02).

We used liposomes to deliver the 5-PCP-$InsP_7$ bioisostere of 5-$InsP_7$ into WT HCT116 cells; unlike the natural pyrophosphate bond, the methylenediphosphonate (PCP) moiety is metabolically resistant (39). 5-PCP-$InsP_7$ also closely mimics 5-$InsP_7$–mediated inhibition of NUDT3 activity (Fig. 1*C*). Delivery of 5-PCP-$InsP_7$ into HCT116 cells elevated levels of our four target mRNA substrates for NUDT3: ITGB6, FN1, LCN2, and S100A8 (Fig. 4*C*). 5-PCP-$InsP_7$ did not affect levels of our two negative-control transcripts which are not NUDT3 substrates (mRNAs for ITGAV and NUDT3 itself; Fig. 4*C*). Finally, 5-PCP-$InsP_7$ promoted a >3-fold increase in P-body abundance, compared with cells treated with "empty" liposomes (Fig. 4 *D* and *E*). These data consolidate our discovery of a role for $InsP_7$ in regulating NUDT3 activity and P-body dynamics.

Concluding Comments. Our data, generated using a complementary series of genetic, pharmacological, and chemical tools, have demonstrated that the small-molecule cell signal 5-$InsP_7$ modulates P-body dynamics and stabilizes a subset of mRNAs that are substrates for NUDT3-mediated mRNA 5′ decapping. To derive these conclusions, we have studied the effects upon mRNA turnover and P-body dynamics of two- to threefold changes in total cellular levels of 5-$InsP_7$. This is a biologically relevant experimental paradigm: A quantitatively similar increase in 5-$InsP_7$ levels has been described during cell stimulation by either insulin or insulin-like growth factor-1 (40). The levels of 5-$InsP_7$ are also >2-fold elevated in both primary hepatocytes and primary bone marrow-derived mesenchymal stem cells prepared from aged mice, as compared with corresponding cells derived from young animals (40, 41); thus, it is particularly

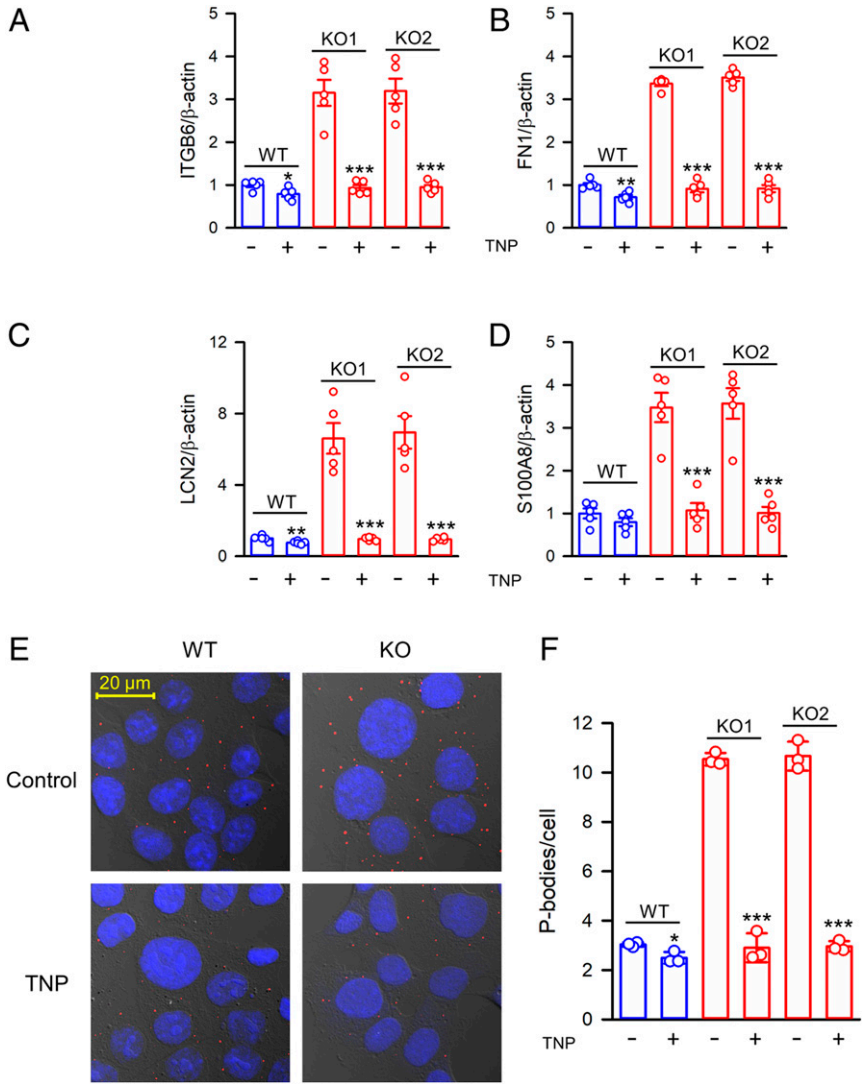

Fig. 3. Effects of TNP upon levels of mRNA transcripts and P-body abundance in WT and *PPIP5K* KO HCT116 cells. WT cells (blue bars) and two independent clones of *PPIP5K* KO cells (KO1 and KO2; red bars) were each treated with either 10 μM TNP (plus sign) or vehicle (minus sign) and then the following data were obtained from these cells. (*A–D*) mRNA transcript levels for ITGB6, FN1, LCN2, and S100A8, respectively, determined by quantitative real-time PCR. (*E*) Representative merged, confocal wide-field images from bright-field, Hoechst staining (blue), and DCP1A immunofluorescence to tag P bodies (red). (*F*) Bar graph of P-body numbers per cell; in every biological replicate (three in total; means and SEs are shown), between 220 and 335 cells were analyzed from each of the six separate conditions. $*P < 0.05$, $**P < 0.02$, $***P < 0.001$, compared with WT.

intriguing that aging is also associated with P-body accumulation, as an adaptive response to maintain proteostasis (20). 5-$InsP_7$ levels also fluctuate in response to the bioenergetic status of the cell (i.e., ATP levels) (8); this homeostatic process underlies the role of 5-$InsP_7$ in mediating nutrient stimulation of insulin secretion from pancreatic β-cells (8). Taken together, these various observations rationalize 5-$InsP_7$ as being a rheostatic signaling molecule that mediates cellular adaptations to environmental challenges (5, 6). Thus, our current study unveils an epitranscriptomic control process; we have shown how 5-$InsP_7$ acts in a molecular pathway by which mRNA structure and stability can be modified in response to fluctuations in the extracellular environment.

Previous studies into the molecular basis for the modulation of cellular protein functions by 5-$InsP_7$ have focused on either allosteric regulation or the alternative nonenzymic covalent modification—the so-called protein pyrophosphorylation (5, 6, 42). Since metabolically resistant 5-PCP-$InsP_7$ recapitulates the inhibition of 5′ decapping and accumulation of P bodies that are driven by $InsP_7$ (Figs. 2 *F* and *G*, 3 *E* and F, and 4 *D* and *E*), it is clear that these events do not involve protein pyrophosphorylation (43). Instead, our study uncovers an alternative mechanism of action of 5-$InsP_7$ that is inherently enzymatic in nature: competition for the active site of NUDT3 (Fig. 1 *A–C*). It is of further interest that substrate overlap between 5-$InsP_7$ and the m^7G cap is specific to NUDT3. The other human *NUDT* genes that encode 5-$InsP_7$ phosphatase activities are *NUDT4* [encodes DIPP2α and DIPP2β (44)], *NUDT10* [encodes DIPP3α (45, 46)], and *NUDT11* [encodes DIPP3β (45, 46)], none of which exhibit any significant decapping activities (23). As such, our data demonstrate that the multiple PP-InsP phosphatase activities are not functionally redundant.

P bodies may originate from nucleation of a relatively small number of specific, high-affinity mRNA–protein and protein–protein interactions, which then snowball through the recruitment of many additional constituents through weaker, multivalent interactions (19, 47), ultimately generating mature P bodies that can then accumulate many other mRNAs (17). We have

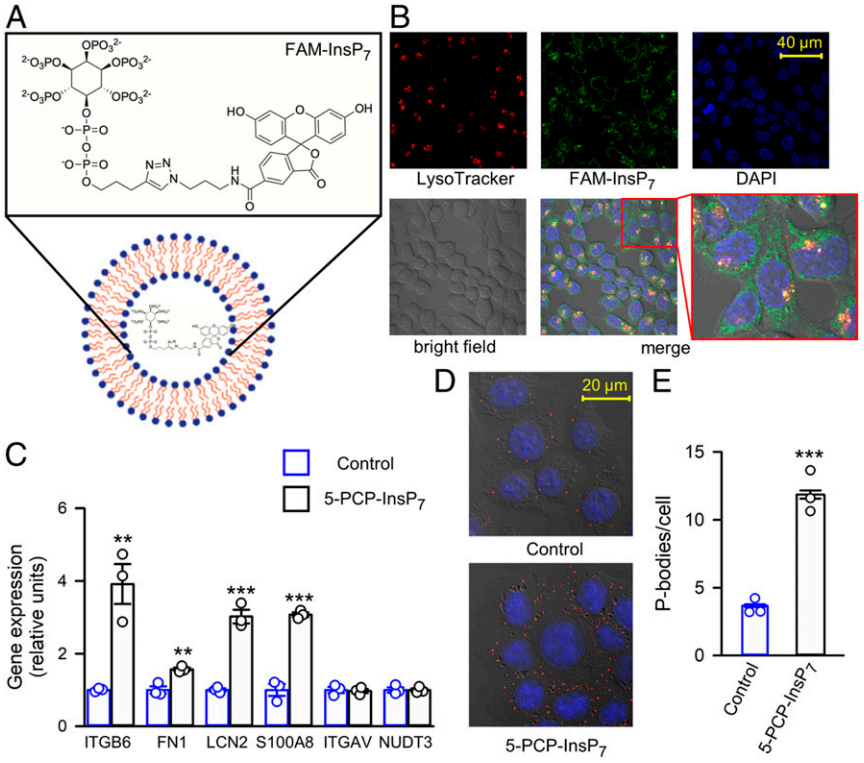

Fig. 4. Liposomal loading of 5-InsP$_7$ analogs into WT HCT116 cells, and their effects upon mRNA transcripts and P-body numbers. (*A*) Graphic depicting the structure of FAM-InsP$_7$ and its incorporation into biocompatible liposomes. (*B*) Analysis of the cellular distribution of FAM-InsP$_7$ after its liposomal loading into cells for 4 h; separate panels are shown for LysoTracker (red), FAM-InsP$_7$ (green), DAPI (blue), and a bright-field image. A merged image is also shown, alongside a magnified area. Data are representative of three biological replicates. (*C*) Levels of the indicated mRNA transcripts, normalized to β-actin, in cells treated for 4 h with either empty liposomes or liposomes containing 5-PCP-InsP$_7$. (*D*) Representative merged, confocal, and wide-field images from bright-field, Hoechst staining (blue), and DCP1A immunofluorescence to tag P bodies (red), obtained from WT cells treated with either empty liposomes ("control") or liposomes containing 5-PCP-InsP$_7$. (*E*) Bar graph of P-body numbers per cell; in every biological replicate (three in total; means and SEs are shown), between 290 and 512 cells were analyzed from each of the two separate conditions. $^{**}P < 0.01$, $^{***}P < 0.001$, compared with WT.

interrogated published datasets to classify 74 NUDT3-responsive mRNAs as P-body constituents (*SI Appendix*, Table S1) that have the potential to be permissive for nascent P-body assembly.

The possibility that 5-InsP$_7$ has other effects that promote P-body accumulation could be a productive direction for future research. If such an event were to occur, it is also possible that an elevation in the numbers of P-bodies, in which mRNAs are stabilized, itself contributes to the elevated levels of those mRNAs that we have utilized as a readout for NUDT3 activity. Such a scenario would represent an indirect, NUDT3-independent effect of 5-InsP$_7$ upon mRNA levels. Nevertheless, our assays of 5-InsP$_7$ levels in WT and NUDT3 knockdown MCF-7 cells (see above) support the idea that NUDT3 can play a direct role in mRNA decapping (4), thereby adding plausibility to our hypothesis that, in appropriate cell types, substrate competition for NUDT3 is permissive for 5-InsP$_7$ to directly regulate mRNA levels. It should be noted there is no evidence that NUDT3 is concentrated in P bodies in either mouse neurons (48), HEK293 cells (17), nor three other human cell lines (https://www.proteinatlas.org/ENSG00000272325-NUDT3). This is not surprising since current data (18) overwhelmingly support P bodies being mainly sites of mRNA storage, not mRNA decapping and decay. Moreover, neither NUDT12 nor DXO decapping enzymes are found in P bodies (17, 49, 50).

There are emerging signs that the functions of P bodies are more wide-ranging than stabilization and storage of mRNA. These noncanonical activities may include mRNA transport, and also sequestration of cell-signaling proteins, for the purposes of their functional silencing and/or protection against proteolysis (51) and as part of an adaptive response to aging (20). There is also interest in the potential therapeutic benefits, particularly with regard to neurodegenerative disorders and stem cell differentiation, if it were possible to intervene in the phase transitions that underlie the turnover of P bodies and other membraneless organelles (18, 19). Our data offer proof of principle that 5′ decapping and P-body fate can be manipulated in a controlled manner by a small regulatory molecule. This is an important step forward toward eventual therapeutic modification of P-body dynamics.

Materials and Methods

Cell Culture. The origins and maintenance of the WT and *PPIP5K* KO cell lines in Dulbecco's modified Eagle's medium (DMEM) supplemented with 10% fetal bovine serum (FBS) (Gemini BenchMark; 100-106) have been described previously (9). For assays of mRNA decay, cells were switched to medium containing 7% FBS for 24 h prior to the experiments. Unless otherwise indicated, all experiments were performed on cells seeded at a density of 2 to 3 × 10^5 per well, in six-well dishes that each contained 2 mL medium; cultures were continued for 2 to 3 d whereupon cells were ∼50% confluent. In some experiments, cells were radiolabeled with [^{3}H]inositol to determine intracellular levels of InsP$_6$ and the PP-InsPs, as previously described (9).

Sources of PP-InsPs and Derivatives. 1-InsP$_7$, 5-InsP$_7$, InsP$_8$, and 5-PCP-InsP$_7$ were synthesized as previously described (52–54). The synthesis of FAM-InsP$_7$ will be described in a separate publication.

Quantitative Real-Time PCR. Cells were harvested and rinsed with ice-cold phosphate-buffered saline (PBS), and RNA was extracted using an RNeasy Mini Kit (Qiagen; 74104) according to the manufacturer's protocol. After quantitation, 2 μg of extracted RNA was used for complementary DNA synthesis using the SuperScript III First-Strand Synthesis System (Invitrogen;

18080051), and quantitative real-time PCR analysis was performed. For assays of mRNA decay, cells were switched to culture media containing 7% FBS 24 h prior to the addition of 5 μg/mL actinomycin D.

The following primers were used:

β-Actin: forward, 5′-AGAGCTACGAGCTGCCTGAC-3′,

reverse, 5′-AGCACTGTGTTGGCGTACAG-3′;

FN1: forward, 5′-TGAAAGACCAGCAGAGGCATAAG-3′,

reverse, 5′-CTCATCTCCAACGGCATAATGG-3′;

ITGAV: forward, 5′-ATCGTGAGGTCGAAACAGGA-3′

reverse, 5′-TGGAGCATACTCAACAGTCTTTG-3′;

ITGB6: forward, 5′-GTGGCAAACGGGAACCAATC-3′,

reverse, 5′-TCTAGCAATCTGTGGAAAGGTCT-3′;

LCN2: forward, 5′-GTTACCTCGTCCGAGTGGTG-3′,

reverse, 5′-TTGGTTCTCCCGTAGAGGGT-3′;

NUDT3: forward, 5′-GAAGCACAGGACGTATGTCTATG-3′

reverse, 5′-CTGCACGGGTTTGTGATACTG-3′;

S100A8: forward, 5′-AGGGGAATTTCCATGCCGTC-3′,

reverse, 5′-CACGCCCATCTTTATCACCAG-3′.

siRNA Protocol. Dharmacon SMARTpool ON-TARGETplus siRNAs were added to cells cultured in six-well plates (30 pmol IP6K1 siRNA [L-006737] and 30 pmol IP6K2 siRNA [L-006738]), using 3 μL of the transfection reagent Lipofectamine 3000 (Invitrogen; L3000015) in 100 μL of Opti-MEM reduced serum medium (Gibco; 31985070). Control cells were transfected with Dharmacon ON-TARGETplus GAPD Control Pool (D-001830-10). The transfection was repeated after 24 h, and cells were analyzed at 48 h.

Assays for 5′ Decapping In Vitro. The decapping assays were performed at 37 °C in 20 μL of assay buffer containing 100 mM potassium acetate, 2 mM magnesium acetate, 2 mM dithiothreitol, 10 mM Tris·HCl (pH 7.5), 0.1 pmol $mG^{32}pppG$-RNA, plus 100 nM recombinant human NUDT3/DIPP1 (unless otherwise stated). Assays were quenched and analyzed by thin-layer chromatography as previously described (23).

Western Blotting and Analysis. Cells were harvested and rinsed with ice-cold PBS, and then a protein extract was prepared using RIPA Lysis and Extraction Buffer (Thermo Fisher Scientific; 89901) supplemented with 1% (volume [vol]/vol) protease-phosphatase inhibitor mixture (Thermo Fisher Scientific; 78442). After quantification with a Pierce BCA Protein Assay Kit (Thermo Fisher Scientific; 23221), 25 μg of each protein extract was resolved by sodium dodecyl sulfate/PAGE, transferred to a polyvinylidene difluoride membrane, and probed with the following primary antibodies: rabbit anti-ITGB6 (Abcam; ab187155; 1:500), rabbit anti-FN1 (Abcam; ab2413; 1:1,000), rabbit anti-LCN2 (Abcam; ab63929; 1:500), sheep anti-S100A8 (R&D Systems; AF4570; 1:500), rabbit anti-IP6K1 (Sigma Prestige Antibodies; HPA040825; 1:500), mouse anti-IP6K2 (Santa Cruz; sc-373770; 1:500), and mouse anti–β-actin (Santa Cruz; sc-47778; 1:5,000). Secondary antibodies were as follows: anti-rabbit immunoglobulin G (IgG) (Invitrogen; 31460; 1:5,000), anti-sheep IgG (Sigma; A3415; 1:5,000), and anti-mouse IgG (Cell Signaling Technology; 7076S; 1:5,000). The immunoblots were developed using SuperSignal West Pico PLUS Chemiluminescent Substrate (Thermo Fisher Scientific; 34580). The blots were scanned using an Odyssey Fc imaging system and software (Li-Cor Biosciences). Densitometric analysis of the protein bands was performed using ImageJ (https://imagej.nih.gov/ij).

Preparation of Liposomes Containing PP-InsP Analogs. Liposomes were prepared as a lipid film inside a round-bottom glass flask, exactly as described previously (9). As needed, the lipid film was hydrated (with vortexing) by the addition of 2 mL 5 mM Hepes (pH 7.2 with NaOH; prepared from a 1 M stock solution; Affymetrix; 16924), plus either 5-PCP-$InsP_7$ or FAM-$InsP_7$. For controls, a corresponding lipid film was prepared without the addition of any PP-InsP. The liposomal dispersion was subjected to five freeze/thaw cycles: freezing at −80 °C for 30 min and thawing at 45 °C for 5 min. The liposomes were then sequentially extruded through two membrane filters, with pore sizes of 0.45 μm and then 0.2 μm and stored in aliquots at 4 °C for up to 2 wk.

P-Body Counting. Cells were grown on 1.5-cm glass coverslips in six-well dishes to ∼50% confluency (0.6 to 0.7 × 10^6 cells per well) in 2 mL DMEM. Where indicated, cells were treated with either siRNA against IP6K (see above) or 10 μM TNP (9), or 2 μL liposomes containing 5-PCP-$InsP_7$. In the latter case, culture medium was switched to inorganic phosphate-free DMEM plus 10% FBS immediately prior to liposome addition. Following the experimental treatments, the medium was aspirated and cells were washed with ice-cold PBS prior to fixation with 3.7% formaldehyde (Macron Chemicals; 5016) dissolved in PBS plus 1 mM $CaCl_2$ and 0.5 mM $MgCl_2$ (PBS+). Fixed cells were washed three times with PBS+/0.02% Triton X-100 followed by PBS+/0.1% Triton X-100. After removal of the permeabilization solution, cells were incubated for 30 min with blocking solution (PBS+/0.02% Triton X-100, 10% donkey serum [Sigma-Aldrich; D9663], 1% BSA [Fisher BioReagents; BP-9703]). Then, the cells on the coverglasses were incubated for 1 h with a P-body marker, rabbit anti-DCP1A antibody (Santa Cruz; sc-100706; 1:200) (12). After subsequent washing of the samples, they were treated with Alexa Fluor 594 donkey anti-mouse secondary antibody (Invitrogen; A21203; 1:1,200) for 1 h at room temperature. After further washing, the coverglasses were mounted on glass slides with ProLong Glass Antifade with NucBlue (Invitrogen; P36985) and sealed. Coverglasses were allowed to cure overnight prior to imaging using an LSM 780 confocal microscope (Carl Zeiss). The 594-nm laser line from an He-Ne laser was used for excitation of the Alexa Fluor 594-conjugated secondary antibody. Fluorescence images were captured using a 40× objective. The 405-nm laser line from a diode laser was used for excitation of the nuclear stain. Images were merged and processed in Zeiss Zen Black software. Both the P bodies and the nuclei were counted using the SPOT function in Imaris software (version 9.2.0) (www.bitplane.com). For quality control purposes, one additional set of experiments (P-body counting in WT vs. KO1 and KO2 HCT116 cells; 230 to 308 cells per condition; these data are not included in the figures) was performed by two researchers independently. Each researcher performed P-body counts on the other's samples in a double blind manner, from confocal fields of view (14 or 15 for each sample) that were selected by a third individual who was unaware of the experimental goal. Statistically similar pairs of P-body counts per cell were obtained: WT, 2.5 ± 0.18 and 2.4 ± 0.09, $P = 0.54$; KO1, 6.6 ± 0.3 and 7.2 ± 0.4, $P = 0.28$; KO2, 7.3 ± 0.37 and 7.9 ± 0.4, $P = 0.25$.

Assessment of Liposomal Delivery of FAM-$InsP_7$ into HCT116 Cells. After liposomal loading of FAM-$InsP_7$ into cells (as described above for 5-PCP-$InsP_7$), cells were washed with PBS twice and then stained by LysoTracker red at 37 °C for 20 min. Subsequently, the cells were washed with PBS twice and stained by Hoechst 33258 at 37 °C for 20 min. After further washing with PBS, the cells were immediately analyzed by confocal microscopy. Images were taken with a Zeiss LSM 780 using the following excitation/emission pairs: 405 nm/415 to 491 nm (for Hoechst), 488 nm/491 to 571 nm (for FAM-$InsP_7$), and 594 nm/597 to 686 nm (for LysoTracker red). A Plan-APOCHROMAT 63×/1.4 oil differential interference contrast objective was used, along with a pinhole setting which yields an optical slice of 0.9 μm. Weighted colocalization coefficients were calculated using Zeiss Zen Black software to describe the number of green pixels (FAM-$InsP_7$) that colocalize with red pixels (LysoTracker), divided by the total number of red pixels.

In some experiments, FAM-$InsP_7$ loading was studied by PAGE analysis. Here, two 150-mm plates, each containing ∼2 to 3 × 10^7 cells, were cultured in 8 mL medium and 240 μL FAM-$InsP_7$ liposomes was added. After 4 h, cells were then quenched by aspiration of culture medium, followed immediately by the addition of 2 mL of 1 M ice-cold perchloric acid; all remaining procedures were performed at 0 to 4 °C. After 45 min, samples from each culture dish were divided between two 1.5-mL tubes and centrifuged at 13,000 rpm, 4 °C for 3 min to eliminate cell debris; the supernatants were transferred to clean microcentrifuge tubes, each containing 5 mg of acid-washed TiO_2 beads (GL Sciences; 5020-75000). The tubes were rotated for 1 h and centrifuged, and the supernatants were discarded. The beads were washed once using ice-cold water, and then the PP-InsPs were eluted with two washes of 10% NH_4OH (55). The NH_4OH was then lyophilized to a volume of ∼50 μL; during the latter step, we combined supernatants derived from samples that originated from each pair of culture plates.

For the PAGE analysis (performed at 4 °C), 31.7% polyacrylamide gels were freshly prepared from the following: 55.5 mL 19:1 (vol/vol) 40% acrylamide:bis-acrylamide (IBI Scientific), 7 mL 10× Tris/borate/ethylenediaminetetraacetic acid (EDTA) buffer, 7.5 mL water, 262 μL ammonium persulfate, and 30 μL tetramethylethylene-diamine. The running buffer was 0.5× Tris/borate/EDTA. A Hoefer 660 tall standard dual-cooled vertical unit was used as the electrophoresis system. The gel was prerun for 1 to 2 h at 200 V, and then the gel lanes were loaded with cell extracts (50 μL; prepared as described above) plus 12.5 μL 6× orange G dye. The gel was run at 300 V

for ∼1 h, until the dye front entered the gel. The gel was then run at 400 V for 18 to 20 h. Gels were stained for 30 min with a mixture of 0.05% (weight [wt]/vol) toluidine blue (Sigma-Aldrich), 20% (wt/vol) methanol, 2% (wt/vol) glycerol in water, and then destained for 2 h with two or three changes of 20% (wt/vol) methanol, 2% (wt/vol) glycerol in water.

Wound Healing Assay. Cells were cultured in six-well plates and scratch-wound healing assays were carried out as previously described, using mitomycin C (Sigma; 1444707) to inhibit cell division (4). The wound gaps were measured with ImageJ software and averaged from at least 15 individual wounds. The data are presented as a percentage of gap closure over time.

Other Materials. Actinomycin D was purchased from Sigma-Aldrich and used at a final concentration of 5 μg/mL. For the 5′-decapping assays, we produced 5′ end-capped RNA labeled at the α-phosphate (relative to the 5′-terminal guanine; i.e., mG^{32}pppG-RNA), as previously described (56); the RNA was purified by passing it through a G-50 column (GE Healthcare). Recombinant NUDT3 was prepared as previously described (57). Recombinant 6×His-tagged NUDT3 in DH5α *Escherichia coli* cells was expressed and the enzyme was purified as previously described (58).

Note Added In Proof. Consistent with our data, A. Shar and R. Bhandari have recently described that P-body formation is stimulated by 5-InsP$_7$ (bioRxiv doi: 10.1101/2020.07.13.199828) (59). Interestingly, in other experiments with their model (U-2 OS cells) Shar and Bhandari show that IP6K1 participates in non-catalytic protein-protein interactions that promotes DCP-dependent mRNA decapping, while we have shown 5-InsP$_7$ inhibits decapping by NUDT3. In the context that the different decapping enzymes DCP2 and NUDT3 are each believed to have their own mRNA substrate specificities and distinct modulatory mechanisms (2), it is intriguing that IP6K1 can regulate each mRNA processing pathway in opposite directions.

Data Availability. All data, associated protocols, methods, and sources of materials can be accessed in the text or *SI Appendix*.

ACKNOWLEDGMENTS. This research was supported by the Intramural Research Program of the NIH, National Institute of Environmental Health Sciences, NIH GM126488 (to M.K.), Swiss National Foundation SNF-170925 (to S.H.), and Deutsche Forschungsgemeinschaft (DFG) under Germany's Excellence Strategy (CIBSS–EXC-2189–Project ID 390939984). H.J.J. additionally acknowledges financial support from the DFG (Grant JE 572/4-1). We also thank Erica Scappini and Charles J. Tucker (NIEHS fluorescent microscopy and imaging core) for their assistance with confocal microscopy and P-body counting.

1. J. S. Mugridge, J. Coller, J. D. Gross, Structural and molecular mechanisms for the control of eukaryotic 5′-3′ mRNA decay. *Nat. Struct. Mol. Biol.* **25**, 1077–1085 (2018).
2. E. Grudzien-Nogalska, M. Kiledjian, New insights into decapping enzymes and selective mRNA decay. *Wiley Interdiscip. Rev. RNA* **8**, e1379 (2017).
3. S. Kramer, A. G. McLennan, The complex enzymology of mRNA decapping: Enzymes of four classes cleave pyrophosphate bonds. *Wiley Interdiscip. Rev. RNA* **10**, e1511 (2019).
4. E. Grudzien-Nogalska, X. Jiao, M. G. Song, R. P. Hart, M. Kiledjian, Nudt3 is an mRNA decapping enzyme that modulates cell migration. *RNA* **22**, 773–781 (2016).
5. A. Chakraborty, The inositol pyrophosphate pathway in health and diseases. *Biol. Rev. Camb. Philos. Soc.* **93**, 1203–1227 (2018).
6. S. B. Shears, Intimate connections: Inositol pyrophosphates at the interface of metabolic regulation and cell signaling. *J. Cell. Physiol.* **233**, 1897–1912 (2018).
7. A. P. Gomes, J. Blenis, A nexus for cellular homeostasis: The interplay between metabolic and signal transduction pathways. *Curr. Opin. Biotechnol.* **34**, 110–117 (2015).
8. S. S. Rajasekaran *et al*., Inositol hexakisphosphate kinase 1 is a metabolic sensor in pancreatic β-cells. *Cell. Signal.* **46**, 120–128 (2018).
9. C. Gu *et al*., KO of 5-InsP$_7$ kinase activity transforms the HCT116 colon cancer cell line into a hypermetabolic, growth-inhibited phenotype. *Proc. Natl. Acad. Sci. U.S.A.* **114**, 11968–11973 (2017).
10. S. T. Safrany *et al*., A novel context for the "MutT" module, a guardian of cell integrity, in a diphosphoinositol polyphosphate phosphohydrolase. *EMBO J.* **17**, 6599–6607 (1998).
11. N. Standart, D. Weil, P-bodies: Cytosolic droplets for coordinated mRNA storage. *Trends Genet.* **34**, 612–626 (2018).
12. A. Aizer *et al*., Quantifying mRNA targeting to P-bodies in living human cells reveals their dual role in mRNA decay and storage. *J. Cell Sci.* **127**, 4443–4456 (2014).
13. W. van Leeuwen, C. Rabouille, Cellular stress leads to the formation of membraneless stress assemblies in eukaryotic cells. *Traffic* **20**, 623–638 (2019).
14. C. Wang *et al*., Context-dependent deposition and regulation of mRNAs in P-bodies. *eLife* **7**, e29815 (2018).
15. N. Cougot *et al*., Structural organization of the polysomes adjacent to mammalian processing bodies (P-bodies). *RNA Biol.* **10**, 314–320 (2013).
16. S. Schütz, E. R. Nöldeke, R. Sprangers, A synergistic network of interactions promotes the formation of in vitro processing bodies and protects mRNA against decapping. *Nucleic Acids Res.* **45**, 6911–6922 (2017).
17. A. Hubstenberger *et al*., P-body purification reveals the condensation of repressed mRNA regulons. *Mol. Cell* **68**, 144–157.e5 (2017).
18. N. Cougot *et al*., Dendrites of mammalian neurons contain specialized P-body-like structures that respond to neuronal activation. *J. Neurosci.* **28**, 13793–13804 (2008).
19. V. Verdile, E. De Paola, M. P. Paronetto, Aberrant phase transitions: Side effects and novel therapeutic strategies in human disease. *Front. Genet.* **10**, 173 (2019).
20. M. Rieckher, M. Markaki, A. Princz, B. Schumacher, N. Tavernarakis, Maintenance of proteostasis by P body-mediated regulation of eIF4E availability during aging in *Caenorhabditis elegans*. *Cell Rep.* **25**, 199–211.e6 (2018).
21. A. Gaete-Argel, C. L. Márquez, G. P. Barriga, R. Soto-Rifo, F. Valiente-Echeverría, Strategies for success. Viral infections and membraneless organelles. *Front. Cell. Infect. Microbiol.* **9**, 336 (2019).
22. B. Di Stefano *et al*., The RNA helicase DDX6 controls cellular plasticity by modulating P-body homeostasis. *Cell Stem Cell* **25**, 622–638.e13 (2019).
23. M. G. Song, S. Bail, M. Kiledjian, Multiple Nudix family proteins possess mRNA decapping activity. *RNA* **19**, 390–399 (2013).
24. A. G. Thorsell *et al*., Crystal structure of human diphosphoinositol phosphatase 1. *Proteins* **77**, 242–246 (2009).
25. R. S. Kilari, J. D. Weaver, S. B. Shears, S. T. Safrany, Understanding inositol pyrophosphate metabolism and function: Kinetic characterization of the DIPPs. *FEBS Lett.* **587**, 3464–3470 (2013).
26. C. Gu, M. S. C. Wilson, H. J. Jessen, A. Saiardi, S. B. Shears, Inositol pyrophosphate profiling of two HCT116 cell lines uncovers variation in InsP8 levels. *PLoS One* **11**, e0165286 (2016).
27. J. C. Otto, P. Kelly, S. T. Chiou, J. D. York, Alterations in an inositol phosphate code through synergistic activation of a G protein and inositol phosphate kinases. *Proc. Natl. Acad. Sci. U.S.A.* **104**, 15653–15658 (2007).
28. D. R. Poyner, F. Cooke, M. R. Hanley, D. J. M. Reynolds, P. T. Hawkins, Characterization of metal ion-induced [^{3}H]inositol hexakisphosphate binding to rat cerebellar membranes. *J. Biol. Chem.* **268**, 1032–1038 (1993).
29. T. A. Randall, C. Gu, X. Li, H. Wang, S. B. Shears, A two-way switch for inositol pyrophosphate signaling: Evolutionary history and biological significance of a unique, bifunctional kinase/phosphatase. *Adv. Biol. Regul.* **75**, 100674 (2020).
30. M. R. Macbeth *et al*., Inositol hexakisphosphate is bound in the ADAR2 core and required for RNA editing. *Science* **309**, 1534–1539 (2005).
31. S. Windhorst *et al*., Tumour cells can employ extracellular Ins(1,2,3,4,5,6)P(6) and multiple inositol-polyphosphate phosphatase 1 (MINPP1) dephosphorylation to improve their proliferation. *Biochem. J.* **450**, 115–125 (2013).
32. H. Chi *et al*., Targeted deletion of *Minpp1* provides new insight into the activity of multiple inositol polyphosphate phosphatase in vivo. *Mol. Cell. Biol.* **20**, 6496–6507 (2000).
33. B. Zhang *et al*.; NCI CPTAC, Proteogenomic characterization of human colon and rectal cancer. *Nature* **513**, 382–387 (2014).
34. K. M. Yamada, Fibronectin peptides in cell migration and wound repair. *J. Clin. Invest.* **105**, 1507–1509 (2000).
35. M. S. Wilson, H. J. Jessen, A. Saiardi, The inositol hexakisphosphate kinases IP6K1 and -2 regulate human cellular phosphate homeostasis, including XPR1-mediated phosphate export. *J. Biol. Chem.* **294**, 11597–11608 (2019).
36. N. Kedersha *et al*., Stress granules and processing bodies are dynamically linked sites of mRNP remodeling. *J. Cell Biol.* **169**, 871–884 (2005).
37. U. Padmanabhan, D. E. Dollins, P. C. Fridy, J. D. York, C. P. Downes, Characterization of a selective inhibitor of inositol hexakisphosphate kinases: Use in defining biological roles and metabolic relationships of inositol pyrophosphates. *J. Biol. Chem.* **284**, 10571–10582 (2009).
38. X. Li *et al*., Control of XPR1-dependent cellular phosphate efflux by InsP$_8$ is an exemplar for functionally-exclusive inositol pyrophosphate signaling. *Proc. Natl. Acad. Sci. U.S.A.* **117**, 3568–3574 (2020).
39. M. Wu *et al*., Elucidating diphosphoinositol polyphosphate function with non-hydrolyzable analogues. *Angew. Chem. Int. Ed. Engl.* **53**, 7192–7197 (2014).
40. A. Chakraborty *et al*., Inositol pyrophosphates inhibit Akt signaling, thereby regulating insulin sensitivity and weight gain. *Cell* **143**, 897–910 (2010).
41. Z. Zhang *et al*., Inositol pyrophosphates mediate the effects of aging on bone marrow mesenchymal stem cells by inhibiting Akt signaling. *Stem Cell Res. Ther.* **5**, 33 (2014).
42. A. Saiardi, Protein pyrophosphorylation: Moving forward. *Biochem. J.* **473**, 3765–3768 (2016).
43. R. Bhandari *et al*., Protein pyrophosphorylation by inositol pyrophosphates is a posttranslational event. *Proc. Natl. Acad. Sci. U.S.A.* **104**, 15305–15310 (2007).
44. J. J. Caffrey, S. T. Safrany, X. Yang, S. B. Shears, Discovery of molecular and catalytic diversity among human diphosphoinositol polyphosphate phosphohydrolases: An expanding NUDT family. *J. Biol. Chem.* **275**, 12730–12736 (2000).
45. N. R. Leslie, A. G. McLennan, S. T. Safrany, Cloning and characterisation of hAps1 and hAps2, human diadenosine polyphosphate-metabolising Nudix hydrolases. *BMC Biochem.* **3**, 20 (2002).
46. L. V. Hua, K. Hidaka, X. Pesesse, L. D. Barnes, S. B. Shears, Paralogous murine Nudt10 and Nudt11 genes have differential expression patterns but encode identical proteins that are physiologically competent diphosphoinositol polyphosphate phosphohydrolases. *Biochem. J.* **373**, 81–89 (2003).
47. D. M. Mitrea, R. W. Kriwacki, Phase separation in biology; functional organization of a higher order. *Cell Commun. Signal.* **14**, 1 (2016).

48. J. K. Kim *et al*., Brain somatic mutations in MTOR reveal translational dysregulations underlying intractable focal epilepsy. *J. Clin. Invest.* **129**, 4207–4223 (2019).
49. F. Picard-Jean *et al*., 2′-O-methylation of the mRNA cap protects RNAs from decapping and degradation by DXO. *PLoS One* **13**, e0193804 (2018).
50. H. Wu *et al*., Decapping enzyme NUDT12 partners with BLMH for cytoplasmic surveillance of NAD-capped RNAs. *Cell Rep.* **29**, 4422–4434.e13 (2019).
51. B. Zhang, P. K. Herman, It is all about the process(ing): P-body granules and the regulation of signal transduction. *Curr. Genet.* **66**, 73–77 (2020).
52. I. Pavlovic *et al*., Cellular delivery and photochemical release of a caged inositol-pyrophosphate induces PH-domain translocation in cellulo. *Nat. Commun.* **7**, 10622 (2016).
53. S. Capolicchio, H. Wang, D. T. Thakor, S. B. Shears, H. J. Jessen, Synthesis of densely phosphorylated bis-1,5-diphospho-myo-inositol tetrakisphosphate and its enantiomer by bidirectional P-anhydride formation. *Angew. Chem. Int. Ed. Engl.* **53**, 9508–9511 (2014).
54. M. Wu, B. E. Dul, A. J. Trevisan, D. Fiedler, Synthesis and characterization of non-hydrolysable diphosphoinositol polyphosphate second messengers. *Chem. Sci.* **4**, 405–410 (2013).
55. M. S. Wilson, S. J. Bulley, F. Pisani, R. F. Irvine, A. Saiardi, A novel method for the purification of inositol phosphates from biological samples reveals that no phytate is present in human plasma or urine. *Open Biol.* **5**, 150014 (2015).
56. Z. Wang, M. Kiledjian, Functional link between the mammalian exosome and mRNA decapping. *Cell* **107**, 751–762 (2001).
57. X. Yang, S. T. Safrany, S. B. Shears, Site-directed mutagenesis of DIPP, a dual specificity MutT/Nudix-type hydrolase that attacks diadenosine polyphosphates and diphosphoinositol polyphosphates. *J. Biol. Chem.* **274**, 35434–35440 (1999).
58. S. W. Liu, X. Jiao, S. Welch, M. Kiledjian, Analysis of mRNA decapping. *Methods Enzymol.* **448**, 3–21 (2008).
59. A. Shah, R. Bhandari, IP6K1 upregulates the formation of processing bodies by promoting proteome remodeling on the mRNA cap. *bioRxiv*:10.1101/2020.07.13.199828 (13 July 2020).